Environmental Science & Technology

Article

pubs.acs.org/est

# Physico-Chemical Heterogeneity of Organic-Rich Sediments in the Rifle Aquifer, CO: Impact on Uranium Biogeochemistry

Noémie Janot,[†,#] Juan S. Lezama Pacheco,[†,‡] Don Q. Pham,[†] Timothy M. O'Brien,[†,▽] Debra Hausladen,[‡] Vincent Noël,[†] Florent Lallier,[§,◆] Kate Maher,[∥] Scott Fendorf,[‡] Kenneth H. Williams,[⊥] Philip E. Long,[⊥] and John R. Bargar*[,†]

[†]Stanford Synchrotron Radiation Lightsource, SLAC National Accelerator Laboratory, Menlo Park, California 94025, United States

[‡]Department of Environmental Earth System Science, Stanford University, Stanford, California 94305, United States

[§]Université de Lorraine, Vandœuvre-lès-Nancy, F-54501, France

[∥]Department of Geological Sciences, Stanford University, Stanford, California 94305, United States

[⊥]Earth Sciences Division, Lawrence Berkeley National Laboratory, Berkeley, California 94720, United States

Supporting Information

**ABSTRACT:** The Rifle alluvial aquifer along the Colorado River in west central Colorado contains fine-grained, diffusion-limited sediment lenses that are substantially enriched in organic carbon and sulfides, as well as uranium, from previous milling operations. These naturally reduced zones (NRZs) coincide spatially with a persistent uranium groundwater plume. There is concern that uranium release from NRZs is contributing to plume persistence or will do so in the future. To better define the physical extent, heterogeneity and biogeochemistry of these NRZs, we investigated sediment cores from five neighboring wells. The main NRZ body exhibited uranium concentrations up to 100 mg/kg U as U(IV) and contains ca. 286 g of U in total. Uranium accumulated only in areas where organic carbon and reduced sulfur (as iron sulfides) were present, emphasizing the importance of sulfate-reducing conditions to uranium retention and the essential role of organic matter. NRZs further exhibited centimeter-scale variations in both redox status and particle size. Mackinawite, greigite, pyrite and sulfate coexist in the sediments, indicating that dynamic redox cycling occurs within NRZs and that their internal portions can be seasonally oxidized. We show that oxidative U(VI) release to the aquifer has the potential to sustain a groundwater contaminant plume for centuries. NRZs, known to exist in other uranium-contaminated aquifers, may be regionally important to uranium persistence.

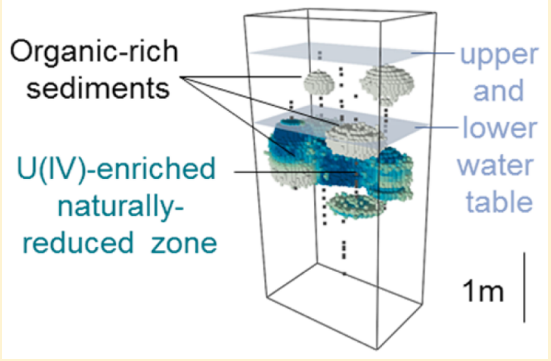


## INTRODUCTION

At U.S. Department of Energy (DOE) legacy uranium ore processing sites across the Colorado River Basin (CRB) (e.g., Rifle and Naturita, CO[1,2]), contaminated surface materials have been removed but aquifer contamination has subsequently persisted for decades. The mechanisms of plume persistence are unknown, but suspicion has fallen on slow pervasive uranium release from fine-grained, sulfidic sediment lenses (i.e., naturally reduced zones, NRZs) that are enriched in uranium.[2] In order for NRZs to contribute to persistent plumes, they must contain sufficient uranium inventories to sustain releases and exhibit both physical and biogeochemical conditions conducive for oxidation. Reduced U(IV) is relatively immobile, providing a mechanism for its accumulation in reduced sediments, whereas oxidized U(VI) is soluble and highly mobile in Rifle groundwater.[3] Consequently, redox zonation within sediments controls uranium speciation, mobility, and concentration. NRZs have been observed in multiple uranium-contaminated aquifers within the upper CRB and exhibit uranium concentrations (up to 48 $mg_U/kg$[4,5]) significantly higher than found in the bulk sediments in the surrounding aquifer (ca. 1 $mg_U/kg$). A robust understanding of redox heterogeneity, biogeochemical processes, and transport processes in NRZs is necessary in order to assess the importance of NRZs to uranium plume persistence in these floodplain aquifers.

Campbell et al. (2012) concluded that the lower permeability of NRZs observed at the former uranium ore processing site at Rifle, CO, creates biogeochemical conditions favorable for microbial reduction of iron, sulfur, and uranium. The spatial resolution of this former study, however, was relatively coarse (1 m vertical intervals). Detailed observations by our group during coring activities at the Rifle site in 2011 showed that NRZs are layered at the cm scale and exhibit textural and compositional heterogeneity over length scales down to ca. 1

Received: July 2, 2015
Revised: November 16, 2015
Accepted: November 25, 2015
Published: November 25, 2015





DOI: 10.1021/acs.est.5b03208
Environ. Sci. Technol. 2016, 50, 46−53

mm, a finer spatial scale than previous reports. Therefore, more detailed qualitative and quantitative information on the physical and biogeochemical attributes of NRZ sediments are needed.

The purposes of this study were (i) to map redox zoning of Rifle sediments across NRZs at scales fine enough to help understand their impact on uranium biogeochemistry and (ii) to better estimate NRZs dimensions as well as the sizes of the pools of reduced uranium, sulfide, and organic carbon. Such information supports the development of improved geochemical models of uranium mobility and floodplain biogeochemical function. To achieve these objectives, five cores were drilled through a previously observed NRZ,[4] sampled at a vertical resolution of about 10 cm, and analyzed using a suite of techniques.

## MATERIALS AND METHODS

**Site Description.** The Rifle field research site is a DOE-managed former uranium and vanadium ore processing mill facility near the town of Rifle, CO, as described elsewhere.[2,3,6−8] Between 1992 and 1996, uranium-rich mill tailings and contaminated soil were removed to a depth of ∼1.6 m and replaced with clean compacted clay fill as part of the Uranium Mill Tailings Remedial Action (UMTRA). However, uranium levels in groundwater have not decreased significantly since 1999, and some estimates suggest they will remain above regulatory limits (0.044 $mg_U/L$) for tens if not hundreds of years.[2,3,9]

**Sediment Collection.** Five sediment cores (150 mm diameter), labeled JB-01 to JB-05, were collected in proximity to the pre-existing well P-103 in a known NRZ[4] (Figure S1 in Supporting Information). Sediments were collected from the depth of the base of the clean sediment cap (1.8 m below ground surface (bgs)) down to bedrock (ca. 5.8 m bgs) across multiple wells at relatively fine vertical resolution (∼10 cm). Sediments from the five JB wells were excavated using a rotosonic drill, encapsulated immediately into $N_2$-purged low density polyethylene sleeves, each approximately 0.7 m in length, and moved into the on-site research laboratory on July 22−24, 2011. Pebbles and cobbles larger than about 10 mm, which accounted for ca. 90% of the mass, were removed, and the remaining sediments were immediately placed into containers. Sediments that were visibly reduced, as identified by the presence of dark coloration, fine grain sizes and sulfidic smell, were collected at ca. 10 cm intervals and rapidly packed into glass jars. Voids were compacted to minimize entrapment of air, the shallow headspaces were immediately covered with groundwater to the top of the jar to exclude air, and metal canning jar lids were affixed. Sand-size and gravelly sediments that did not visually display evidence of reduction were sealed into $N_2$-purged double aluminized Mylar bags with oxygen absorbers. Sediments were shipped within 72 h of collection to the SLAC National Accelerator Laboratory where they were stored at 3 °C until analysis. During all subsequent sample manipulation and preparation steps, glass jars were opened in an anaerobic chamber to avoid oxidation of the material. Subsamples taken after homogenization of the material within the glass jar were then either dried inside the anaerobic chamber before spectroscopic analysis or air-dried for total elemental composition analysis. The samples analyzed in this study represent the <2 mm size fraction of these sediments.

**Elemental Composition Analysis.** For each sample, ∼20 g of sediment were subsampled (after homogenization of the jar material) and air-dried. After drying, samples were sieved and the <2 mm size fraction was ground using a shatterbox with WC vessels for 2 min.

X-ray fluorescence (XRF) analyses were conducted with a Spectro Xepos instrument on ∼4 g of powdered sediments at Environmental Measurement I (EM-1) laboratory at Stanford University, CA.

Solid phase carbon (total and organic) was measured using an elemental analyzer (EA) Carbo Erba NA1500. Around 30 mg of ground sample was weighed in tin cups. For organic carbon (OC) measurements, samples were acidified with 2 drops of 8% $H_3PO_4$ and allowed to degas overnight in order to remove inorganic carbonates before analysis.

A subset of selected samples were dried and ∼100 g of the <2 mm fraction was sieved into 5 fractions using a standard series of mesh sizes for 10 min. Sieving was performed using a set of 3" stainless steel and brass nested sieves (53 μm, 150 μm, 500 μm, 1 mm, 2 mm) by hand shaking. Size fractions were collected and analyzed for elemental composition.

**Carbon Dating.** Subsets of sediments were shipped to Beta Analytics for radiocarbon dating measurements on fine root, woody fragments and plant material. Radiocarbon dating was determined by the accelerator mass spectrometry (AMS) method measuring directly the amount of $^{14}C$ in the sample.

**Spectroscopy Analysis.** Sulfur K-edge X-ray absorption spectroscopy (XAS) were measured from wet anoxic sediments to map the distribution of sulfur oxidation states. Uranium XAS was used to determine the oxidation state and molecular structure around uranium. Data collection and analysis operations are described in the Supporting Information.

## RESULTS

**Sediment Texture and Color.** Textures and colors of cored sediments were highly variable. A summary of sediment descriptions is provided in Table S1. Most of the cores were comprised of oblate spheroidal siliciclastic cobbles larger than 5 cm diameter (with major axis ≤20 cm), pebbles, gravel, and sand exhibiting a light brown color. Fine-grained sediment was commonly present as thin layers interleaved between and infilling interstices created by cobbles (Figure 1). Within fine-grained sediments, redox zonation was apparent from brown-to-black color contrasts defined by sharp boundaries, indicating local areas of sulfate reduction and precipitation of dark-colored metal sulfides. These darker fine-grained materials were observed in lenses at different depths in the different cores: at 4.0−4.5 m bgs in JB-01, at 4.0−4.3 m bgs and 5.5 m bgs in JB-02, 3.8−4.6 m bgs in JB-04, at 3.5−3.7 and 3.8−4.1 m bgs in JB-05, whereas none were observed in JB-03.

**Vertical and Horizontal Distributions of Trace and Minor Elements.** Sulfur, uranium and OC concentration profiles in the five JB cores are shown in Figure 2. Well-defined layers of high concentrations were present, with sharp variations at the centimeter scale. For example, in well JB-02, U and OC concentrations increase from 13 mg/kg and 0.3 wt %, respectively, to 55 mg/kg and 1.0 wt % between 4.4 and 4.5 m bgs.

Zones of elevated sulfur, OC, and uranium exhibit variable thicknesses and were found at different depths in the different JB wells. In well JB-01, we observed a zone enriched in U/S/OC at 3.5−4.0 m bgs. In well JB-02, this layer occurred at 4.0−4.5 m bgs (which coincides with the black fine-grained sediments observed during sample collection, Table S1) and contained up to 102 $mg_U/kg$ (4.3 m bgs). This value is higher than any previously reported natural concentrations of uranium


DOI: 10.1021/acs.est.5b03208
Environ. Sci. Technol. 2016, 50, 46−53

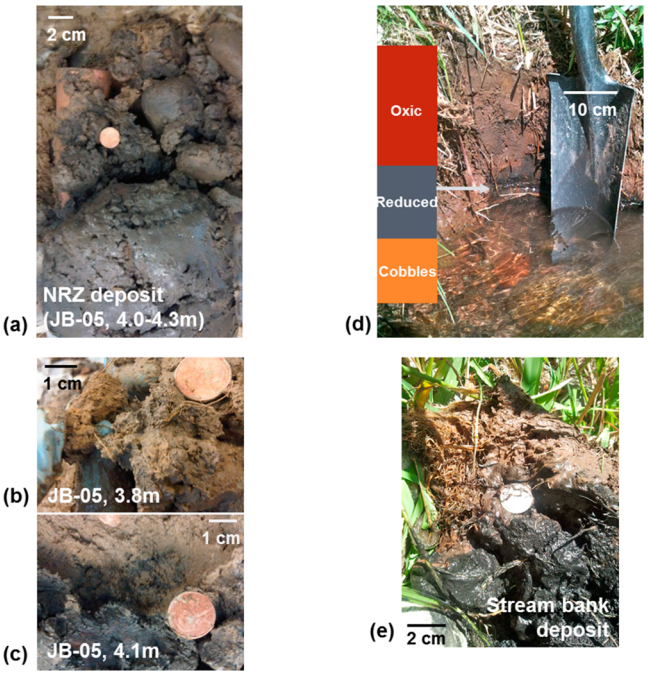


**Figure 1.** Pictures of Rifle sediments (left, a–c) and nearby contemporaneous river bank deposits (right, d–e, Roaring Fork river, Basalt, CO). Rifle sediments from well JB-05 (a) contain abundant large cobbles with reduced clay/silt in between. Sediment details are shown for Rifle organic-rich sediments (JB-05, b–c) and stream bank deposits (e). Note the presence of fine roots and sharp redox boundaries in both NRZs and river-bank deposits (b and e, respectively).

reported for the upper CRB to our knowledge: acid-extractable concentrations up to 64 $mg_U/kg$ were reported at the Naturita site[1] whereas at Rifle maximum concentrations of 19 $mg_U/kg$[10] and 48 $mg_U/kg$[4] were found in wells D-08 and P-103 (at 4.9 and 3.1 m bgs, respectively). Sediments from JB-01 and JB-02 show up to 1.7% OC, which exceeds previously reported concentrations of 1% (well P-103[4]). In well JB-04, sediments enriched in U/S/OC were present at 3.8–4.6 m bgs, and exhibited variable concentrations. This variability was also observed at the macroscopic scale (Table S1); root material embedded in mottled light and dark sulfidic sediments were present in these samples. In wells JB-03 and JB-05, sediments were less enriched in uranium (≤12 mg/kg and ≤3 mg/kg in JB-03 and -05, respectively) and in OC (≤0.3% and ≤0.9% in JB-03 and -05, respectively).

Total iron concentration depth profiles do not show marked variations (Figure S2), but reduced sediments are slightly enriched in Fe, with concentrations up to 3.3% in JB-02 NRZ when they are at 2.0–2.5% in the background aquifer sediments, in agreement with previous observations.[4] Manganese profiles show similar variations as Fe (Figure S2), with concentrations between 200 and 600 mg/kg.

**Depositional Age.** Radiocarbon dating was performed on detrital organic material (roots, twigs) found in a subset of samples from various wells and depths. Organic carbon ages range from 110 to 180 ± 30 yr BP (calibrated to years before 1950, Figure 2). These dates provide maximum ages for the time of deposition of overlying sediments, assuming that the roots and twigs analyzed have not equilibrated with modern carbon introduced by microbes or modern DOC.

**Redox Variability with Depth.** Figure 3 shows the sulfur K-edge XANES spectra of samples from well JB-02, from 3.2 to 4.5 m bgs. The loss of sulfate as a percentage of total S species with depth is clearly seen, the characteristic 2482 eV peak diminishing in the spectra from sediments below 4.0 m bgs. In deeper samples, spectra show peaks between 2470 and 2475 eV, characteristic of inorganic sulfides (Figure S3). No organic forms of sulfur, whose spectra show peaks between 2473 and 2481 eV,[11] were detected.

Linear combination fitting (LCF) results are shown in Figure 3 (details in Figures S4 and S5) and parameters are summarized in Table S2. The presence of iron sulfides (FeS, $FeS_2$, $Fe_3S_4$)

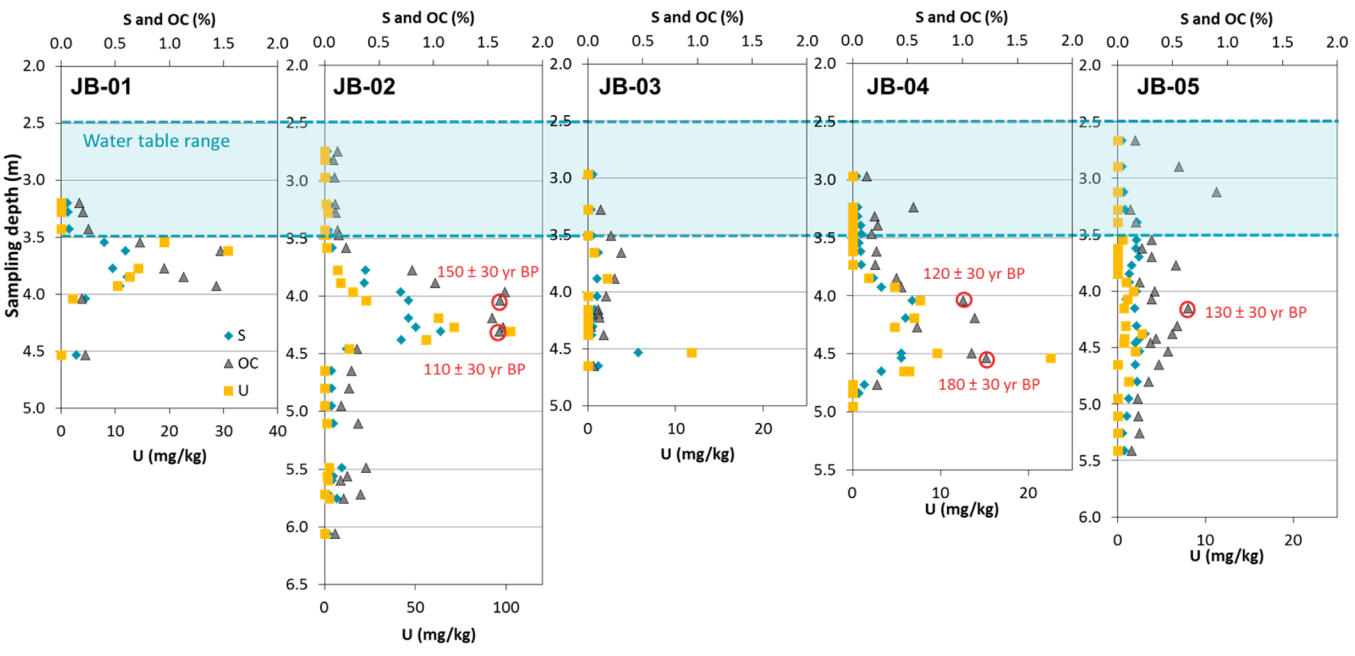


**Figure 2.** Vertical variations of sulfur (diamonds), uranium (squares) and organic carbon (triangles) concentrations in sediment cores JB-01 to JB-05 (left to right). Samples analyzed for radiocarbon dating and results are circled in red.



DOI: 10.1021/acs.est.5b03208
*Environ. Sci. Technol.* 2016, 50, 46–53

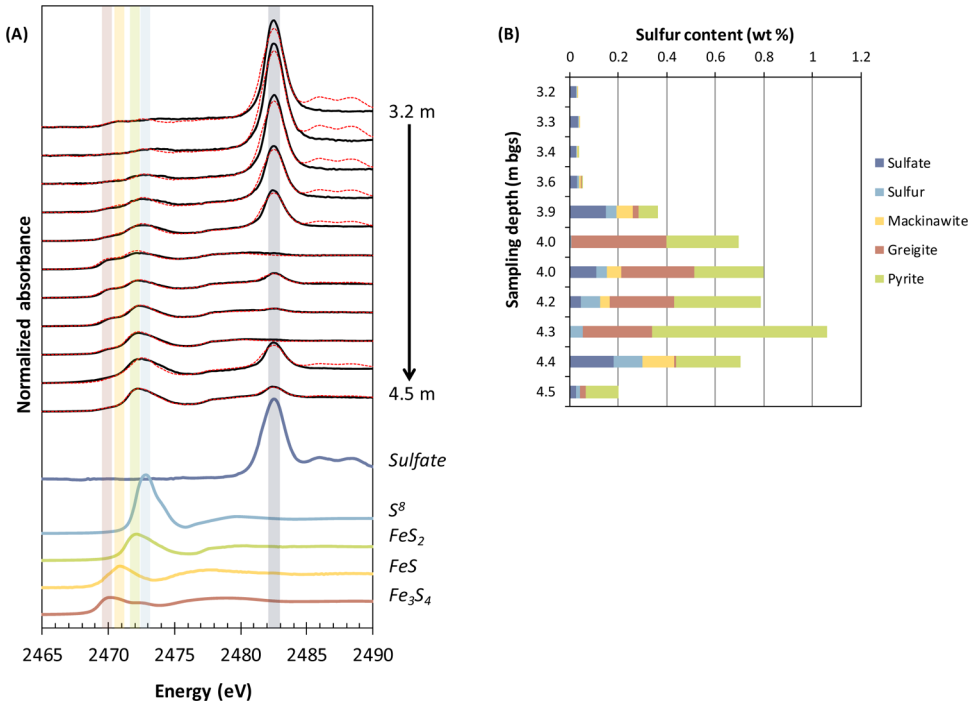


**Figure 3.** (A) Sulfur XANES spectra of natural sediments as a function of depth in well JB-02 (black lines), together with the reference compounds used for linear combination fitting (LCF, colored lines) and fit results (red lines). (B) Decomposition of sulfur speciation estimated from LCF results.

correlates with increasing concentrations of total sulfur species. At the interface with the aquifer (around 3.9 m bgs), reduced sulfur is mainly present in the form of monosulfides (mackinawite and greigite). Greigite was not observed in a previous study using Mössbauer spectroscopy on similar samples,[4] but its absence from the samples could be explained by the spatial variability of its abundance. In contrast, pyrite is the most abundant sulfide in the interior of the NRZ. Detailed results of the LCF are shown in Figure S6 for two of these samples: one from the aquifer (3.4 m bgs), one from the NRZ (4.3 m bgs).

**Sediment Particle Size-Dependence of Sulfur, OC, and Uranium.** Sieving of JB-02 samples showed that fine particles (<53 $\mu$m) are more abundant in NRZs (4.2−4.4 m bgs) than in the surrounding aquifer (Figure S7). The main difference between NRZs and aquifer sediments resides in the proportion of <150 $\mu$m fraction, in agreement with Campbell et al. (2012):[4] in all cases this fraction represents more than 25% of the <2000 $\mu$m fraction, and its proportion reaches 69% in the 4.2 m bgs sample.

Sulfur is most abundant in the smallest size fractions in all analyzed samples (Table 1), but this is not the case for uranium. In the nonreduced samples (3.4 and 3.6 m bgs), we observed that uranium and OC are most abundant in the smallest size fraction. In NRZs, however, uranium is most abundant in the fraction with the most OC, that is, in the 150−500 $\mu$m fraction, in two of the three samples. In these reduced samples, uranium concentration is lowest in the 53−150 $\mu$m fraction. The a priori expectation was that more uranium would be present in the fine- versus the coarse-grained fraction, as reported previously in similar samples.[4] Differences in our results illustrate the substantial heterogeneity in aquifer composition and sampled material.

**Table 1. Uranium, Sulfur and Organic Carbon Contents in Size Fractions of JB-02 Samples**

| | | | U (mg/kg) | S (%) | OC (%) |
|---|---|---|---|---|---|
| aquifer | 3.4 m | bulk | <0.6 | 0.04 | 0.1 |
| | | < 53 $\mu$m | 5 | 0.13 | 1.0 |
| | | 53−150 $\mu$m | 2 | 0.08 | 0.4 |
| | | 150−500 $\mu$m | <0.4 | 0.04 | 0.2 |
| | 3.6 m | bulk | <0.6 | 0.06 | 0.2 |
| | | < 53 $\mu$m | | | |
| | | 53−150 $\mu$m | 6 | 0.18 | 0.8 |
| | | 150−500 $\mu$m | 2 | 0.10 | 0.4 |
| NRZ | 4.2 m | bulk | 74 | 0.79 | 1.5 |
| | | < 53 $\mu$m | 51 | 1.17 | 1.0 |
| | | 53−150 $\mu$m | 46 | 0.92 | 1.0 |
| | | 150−500 $\mu$m | 80 | 0.84 | 2.0 |
| | 4.3 m | bulk | 102 | 1.06 | 1.6 |
| | | < 53 $\mu$m | 101 | 1.13 | 1.6 |
| | | 53−150 $\mu$m | 84 | 0.90 | 1.3 |
| | | 150−500 $\mu$m | 110 | 0.98 | 1.8 |
| | 4.4 m | bulk | 56 | 0.70 | 0.9 |
| | | < 53 $\mu$m | 85 | 1.17 | 1.2 |
| | | 53−150 $\mu$m | 69 | 0.95 | 0.9 |
| | | 150−500 $\mu$m | 79 | 0.74 | 1.3 |

**Uranium Oxidation State and Local Structure.** Uranium $L_{II}$-edge XANES spectra from JB-01 and JB-02 samples are presented in Figure S8. LCF of XANES spectra using uraninite as U(IV) standard and autunite as U(VI) standard gave 100 ± 10% U(IV) in all the JB-02 samples, and 86 ± 10% U(IV) in the JB-01 sample. EXAFS and Fourier Transform of uranium in two JB-02 NRZ samples, 4.2 and 4.3 m bgs, are shown in Figure S9. They are similar to those of U(IV) in a P-103 sample.[4] Results of shell-by-shell fitting are


DOI: 10.1021/acs.est.5b03208
Environ. Sci. Technol. 2016, 50, 46−53

summarized in Table S3. Both spectra show a small second shell frequency around 3.85 Å corresponding to U−U pair correlation, implying minor amounts of $UO_2$ in these sediments, but no U−P pair correlation was detected.

## DISCUSSION

**Compositional Heterogeneity of the Aquifer.** Analysis of the samples shows that the physicochemical and redox conditions of the aquifer differ vertically on a cm scale and laterally on a scale of less than 2 m (Figure S1). We operationally define NRZs as samples with more than 0.35% S. Within the five cores studied here, naturally reduced sediments represent 20% of total analyzed samples and they contain 90% of the total sediment uranium inventory and 56% of the total sediment OC inventory: these structures accumulate large inventories of these elements. In addition, homogenization of sampled material may result in dilution of smaller-scale structures: pictures of JB-05 samples taken during excavation reveal the presence of locally black, reduced sediments (Figure 1) that do not coincide with elevated sulfur concentrations. NRZs identified in this study are thus structures larger than the subdecimeter scale, but it is important to note that smaller structures are also existent.

JB-01, JB-02, and JB-04 each shows a well-defined OC-rich lens with sharp margins (Figure 2), with a top elevation decreasing from 3.5 m to 4.0 m bgs from JB-01 to JB-04 along a SW-NE axis (Figure S1). These three cores seem to belong to a single NRZ structure that thickens between JB-01 and JB-04 and likely extends beyond the boundaries of the well cluster. In comparison, JB-03 and JB-05 exhibit much lower concentrations of OC distributed more diffusely over a broader range of elevations than in the other three cores. These two wells lie on the periphery of the JB-01-02-04 axis, suggesting that they represent the margins of an elongate NRZ body (Figure 5).

Sulfur profiles show well-defined enrichment zones within the main JB-01/02/04 NRZ and are coincident with the OC enrichment profiles (Figure 2). This suggests that OC content helps to control sulfur accumulation in the sediments. However, in cores JB-04 and JB-05, some OC-rich sediments (containing more than 0.5% OC) do not accumulate sulfur (Figure 4). In these two cores, OC-rich, nonsulfidic layers are found above 3.5 m bgs, the average depth of the water table (Figure 5). Present within the capillary fringe, these OC-rich sediments are seasonally exposed to oxygen and thus do not retain reduced sulfur. Low sulfide contents are also observed in permanently saturated parts of the aquifer in JB-05 and JB-02. Sediment textures reported in Table S2 show that organic-rich layers in JB-03 and JB-05 are coarser-grained than in the other cores. In JB-02, core logs indicate a sediment grain-size transition between sandy nonreduced sediments (3.8 m bgs) to silt/clay-sized reduced sediments (4.1 m bgs) which is in agreement with the sharp variation in the sulfur profile shown in Figure 2. Size-fractionated elemental analysis also shows sulfur concentrations increasing with decreasing particle size in each of the analyzed samples (Table 1). These results support the previous conclusions that NRZs accumulate sulfide and uranium, based on their low permeability, higher specific surface areas, smaller particle sizes, and elevated clay and uranium contents.[4] In more permeable sediments, oxygen can be transported faster than it is consumed, and anoxic conditions are difficult to achieve. Thus, sulfur is not reduced to lower-solubility sulfide in coarser sediments.

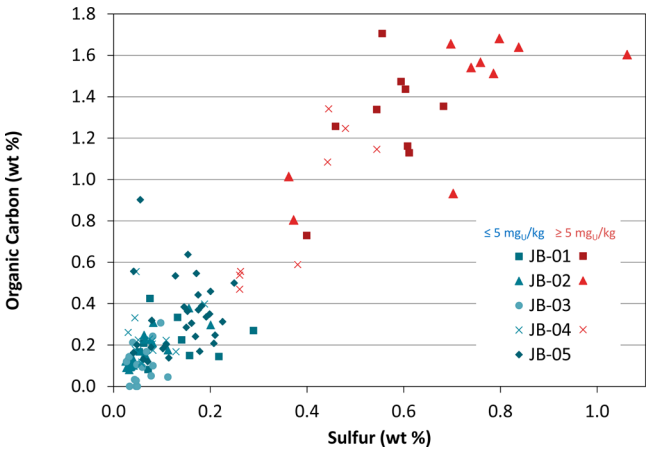


**Figure 4.** Elemental abundances of organic carbon and sulfur in the sediments from wells JB-01 (squares), JB-02 (triangles), JB-03 (circles), JB-04 (crosses), and JB-05 (diamonds). Red symbols: ≥ 5 mg/kg U; blue symbols: ≤ 5 mg/kg U.

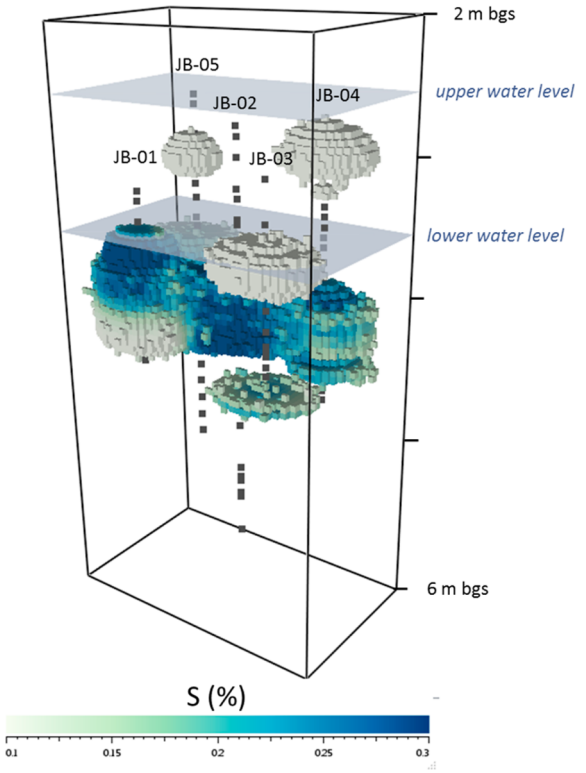


**Figure 5.** Three-dimensional representation of the distribution of organic-rich lenses within the JB well cluster. Delimitation of lenses is based on OC measurements (OC > 0.4%) and macroscopic observations during sample collection. Within these lenses, sulfur concentration is interpolated on a regular grid from S measurements in core samples. White and colored volumes are the nonreduced zones and S-enriched NRZs, respectively.

**Sulfur Biogeochemical Cycling.** Sulfur K-edge XANES measurements of NRZ sediments showed the presence of elemental sulfur and iron monosulfides (mackinawite and mostly greigite) and disulfide (pyrite). Mackinawite, together with elemental sulfur, can be generated from sulfate by microbial activity, as well as by abiotic reduction of Fe(III) minerals coupled to the oxidation of aqueous sulfide.[3,12,13] The



DOI: 10.1021/acs.est.5b03208
Environ. Sci. Technol. 2016, 50, 46−53

presence of these species in NRZ sediments strongly suggests ongoing sulfate reduction in these zones and implies an active mass exchange between the aquifer and the NRZ. Results also show the presence of a significant amount of mackinawite in aquifer sediments in the capillary fringe above the NRZ (Figure S4), indicating that reducing conditions are present in the oxic portion of the aquifer, probably maintained in the interior of aggregates within the organic-rich sediments.

Under low-oxygen conditions, two-thirds of Fe(II) in mackinawite can oxidize, resulting in a solid-state transformation to greigite.[14] The presence of greigite in all NRZ samples, together with the presence of some sulfate in the majority (Figure 3), suggests that NRZs are regularly exposed to oxidants that penetrate through these sediment structures. Elemental sulfur can also be produced from abiotic or biotic FeS oxidation in natural sediments.[15] These observations point to dynamic redox cycling in the aquifer, likely tied to seasonal variations in groundwater elevation that enable sulfate reduction and FeS precipitation during periods of complete saturation and/or low oxygen conditions, and FeS oxidation to $Fe_3S_4$ and sulfate during partially saturated and/or higher oxygen conditions when groundwater elevations seasonally decrease.[16]

The composition of the reduced pool of sulfur varies with depth: near-surface oxidized sediments mostly contain mackinawite whereas pyrite is most abundant in the interior and lower portions of the NRZ (Figure S5). Greigite is most abundant at the NRZ−aquifer interface. This could suggest that greigite is a precursor for pyrite formation from mackinawite, as widely proposed.[10] However, this traditional view is strongly debated, with others suggesting that greigite and pyrite may represent distinct end points of competing Fe−S mineralization pathways.[14,17] In the latter case, differences in the end-point mineralogy may be due to local differences in biomass activity and pore-water $Fe^{2+}$ concentration.[17]

It is known that following sulfate reduction in sediments, aqueous sulfide can undergo reoxidation and react either with organic matter to form organic S species or with reactive ferric species to form iron sulfides.[11,18,19] Our results show that in Rifle NRZs sulfur pairs with iron and forms FeS particles in the fine fraction, whereas OC is most abundant in larger size fractions and no organic S species are detected with XANES analysis. Sulfurization of organic matter is not observed in these sediments to a detectable extent, and instead, the dominant sink for reduced sulfur seems to be iron sulfides. As suggested by Couture et al. (2013), this may be an indicator of the low lability of the OC.[19]

**Biogeochemical Controls on Uranium.** Figure 4 shows that elevated uranium concentrations (red data points) are only found in sediments rich in OC: sediments with more than 5 $mg_U/kg$ contain at least 0.2% S and 0.3% OC. However, OC-rich zones, when not enriched in sulfur (such as occurs in JB-05 core), do not accumulate uranium (Figure S10). This suggests that sulfate-reducing conditions are important for uranium accumulation. These sulfate-reducing conditions were established with the deposition of organic-rich sediments. The railroad was built on the floodplain in its current configuration by 1910. Assuming that the water table was then approximately in its present-day location, the NRZ sediments should have been buried and saturated as of that time, at least 40 years prior to arrival of uranium contamination. Sulfate-reducing conditions should have developed quickly. Consequently, the system is expected to have been sulfidic when dissolved U(VI) began to occur as a contaminant.

In reduced sediments, uranium is relatively more abundant in the largest size fraction (4.2 and 4.3 m) and smallest size fraction (4.4 m) as compared to the intermediate size. Sulfide is most abundant in the smallest size fraction, whereas organic carbon is most abundant in the largest fraction. These results suggest that uranium is associated with both sulfides and with organic carbon (Table 1). These observations suggest that biological activity associated with decomposition of organic matter is important and it is plausible that U(VI) reduction is facilitated by binding to bacterial biomass, as previously proposed.[20] It is also plausible that electron shuttles are more abundant in these organic-enhanced zones and facilitate uranium reduction. Several reduction pathways are likely to be present in these sediments: abiotic reduction by iron sulfides that produce uraninite[21] as well as biological mediation of electron transfer via enzymatic activity.[20]

The abundant sulfides in NRZs are expected to react strongly with dissolved oxygen, protecting uranium from oxidation.[4] Other oxidants that are less reactive with sulfide, such as nitrate, may be more important for uranium oxidation in NRZs, as demonstrated by several authors.[22−25] Nitrate is highly soluble and can diffuse into NRZs to be subsequently reduced to nitrite, a strong oxidant for U(IV),[24−26] by denitrifying bacteria. Williams et al. (2014) have observed nitrate in relatively high (millimolar) concentrations in Rifle porewaters proximal to NRZ sediments during seasonal water level changes[27] and recently Nolan and Weber showed a correlation between uranium and nitrate levels in groundwater in major U.S. aquifers.[28] Further research is required to investigate the possible roles of denitrification and nitrification on uranium accumulation and release.

**Depositional Environment.** Recent papers have noted that deep burial of soil horizons is common in alluvial floodplain sediments[29,30] and contribute large stores of carbon and biological productivity to deep (>30 cm) floodplain sediments.[31,32] If Rifle NRZs are buried soil horizons, then they should share textural characteristics with modern nearby soil horizons. Sediment textures in local river banks were examined to evaluate this hypothesis. Bank sediments from the Roaring fork River, a nearby tributary of the Colorado River, exhibited strong textural similarity to NRZs (Figure 1). The riverbed was paved with cobbles of 50 to >200 mm diameter, common in the upper CRB.[33,34] Riverbank grass mats growing over this cobble surface produced direct contact of fine-grained sediments and roots and underlying cobbles. A sulfidic horizontal redox transition located approximately at the water level (Figure 1), produced sharp juxtaposition of lighter colored and black sulfidic sediments. The presence of these textural features in Rifle NRZ sediments supports the idea that NRZs are buried riverbank soil horizons. It is reasonable to posit that NRZs are present in alluvial floodplains throughout the upper CRB and accumulate uranium wherever it is present in groundwater.

**Environmental Implications.** Storage and release of uranium, OC, and sulfur in NRZs may have a substantial impact on aquifer water quality. NRZ sediments analyzed in this study contain an average of 26 $mg_U/kg$. Based on the inferred dimensions of the main NRZ observed here (4 m long, 2 m wide and about 0.5 m thick), and using a sediment particle density of 2.75 kg/L,[35] the estimated inventory of uranium within the limited area of the study plot is 286 g. The net flux of uranium from the NRZ to the aquifer determines whether this


DOI: 10.1021/acs.est.5b03208
Environ. Sci. Technol. 2016, 50, 46−53

NRZ could sustain a uranium plume. Assuming a steady-state flow system with a fixed flux independent of the concentrations and reaction rates within the NRZ, this flux $J_{NRZ}$ is given by

$$J_{NRZ} = C\frac{\phi h v}{x}$$

where $\phi$ is the porosity (0.15−0.35[36]), $h$ is the saturated thickness of the aquifer (2.4−3.4 m[36]), $v$ is the mean pore water velocity by (109−182 m/yr[36]), and $x$ is the downgradient flow path (138 m from the NRZ to the river). The concentration of U in the groundwater ($C$) is the threshold value used to define a contaminant plume at a given value of $x$. Using this formulation, the flux of U required to maintain plume levels above the UMTRA groundwater remediation standard for uranium of 44 $\mu$g/kg[6] is $J_{NRZ}$ = 13−69 mg/m$^2$/yr. The time interval over which a plume could be maintained, for a simple order-of-magnitude estimate, depends on the inventory of uranium with the NRZ, the interfacial area of the NRZs and the net flux. Assuming 286 g of uranium in the NRZ released to the aquifer through its top and bottom interfaces (a 16 m$^2$ area), then the maximum duration over which a 2m-wide plume could be sustained is 259−1375 years.

Measuring the magnitude of the uranium outward flux from NRZs is difficult and beyond the scope of the present study. Nevertheless, this discussion highlights the need to understand the rates and mechanisms of uranium mass transfer between NRZs and the aquifer under field conditions, the processes that govern the generation of and transport of U within the NRZ, as well as the potential importance of NRZs to plume generation when oxidizing conditions are present. Large climate-driven variations in redox conditions occur seasonally and interseasonally (e.g., multiyear drought cycles).[16] Consequently, oxidation of NRZs is likely to be common, and decreasing rainfall in future seasons would be expected to overall drive uranium release through enhanced oxidation of uranium in the unsaturated zone accompanied by seasonal flushing of U during meltwater discharge events. Because organic-enriched sediments are expected to be common floodplain depositional features, we should expect them to be present in the numerous contaminated floodplain DOE sites in the upper CRB.

## ■ ASSOCIATED CONTENT

### Supporting Information

The Supporting Information is available free of charge on the ACS Publications website at DOI: 10.1021/acs.est.5b03208.

Additional method details, figures, and tables (PDF)

## ■ AUTHOR INFORMATION


### Corresponding Author

*Fax: 650-926-4100; e-mail: bargar@slac.stanford.edu.

### Present Addresses

#(N.J.) Université de Lorraine, LIEC, UMR7360, Vandœuvre-lès-Nancy, F-54501, France.

▽(T.M.O.) Department of Geological Science, Stanford University, Stanford, CA 94305, United States.

◆(F.L.) TOTAL E&P UK Ltd., Altens, Aberdeen AB12 3FG, United Kingdom.


### Notes

The authors declare no competing financial interest.

## ■ ACKNOWLEDGMENTS

The SLAC Scientific Focus Area (SFA) program is supported by U.S. DOE Office of Biological and Environmental Research (BER), Subsurface Biogeochemical Research (SBR) program under subcontract DE-AC02-76SF00515. Logistical support was provided by Rifle field research program at the Lawrence Berkeley National Laboratory through funding from DOE-BER-SBR to the Sustainable Systems SFA 2.0 under contract DE-AC02-05CH11231. We thank Julian Carpenter and Dr. Ritimukta Sarangi for providing FeS and elemental sulfur reference compounds, respectively. Greigite synthesis was developed at the IMPMC (Paris, France).

## ■ REFERENCES


(1) Davis, J. A.; Curtis, G. P.; Wilkins, M. J.; Kohler, M.; Fox, P. M.; Naftz, D. L.; Lloyd, J. R. Processes affecting transport of uranium in a suboxic aquifer. *Phys. Chem. Earth, Parts A/B/C* **2006**, *31* (10−14), 548−555.

(2) Zachara, J. M.; Long, P. E.; Bargar, J. R.; Davis, J. A.; Fox, P. M.; Fredrickson, J. K.; Freshley, M. D.; Konopka, A. E.; Liu, C.; McKinley, J. P.; Rockhold, M. L.; Williams, K. H.; Yabusaki, S. B. Persistence of uranium groundwater plumes: Contrasting mechanisms at two DOE sites in the groundwater-river interaction zone. *J. Contam. Hydrol.* **2013**, *147*, 45−72.

(3) Williams, K. H.; Long, P. E.; Davis, J. A.; Wilkins, M. J.; N'Guessan, A. L.; Steefel, C. I.; Yang, L.; Newcomer, D. R.; Spane, F. A.; Kerkhof, L. J.; McGuinness, L.; Dayvault, R.; Lovley, D. R. Acetate availability and its influence on sustainable bioremediation of uranium-contaminated groundwater. *Geomicrobiol. J.* **2011**, *28* (5−6), 519−539.

(4) Campbell, K. M.; Kukkadapu, R. K.; Qafoku, N. P.; Peacock, A. D.; Lesher, E.; Williams, K. H.; Bargar, J. R.; Wilkins, M. J.; Figueroa, L.; Ranville, J. F.; Davis, J. A.; Long, P. E. Geochemical, mineralogical and microbiological characteristics of sediment from a naturally reduced zone in a uranium-contaminated aquifer. *Appl. Geochem.* **2012**, *27* (8), 1499−1511.

(5) Qafoku, N. P.; Gartman, B. N.; Kukkadapu, R. K.; Arey, B. W.; Williams, K. H.; Mouser, P. J.; Heald, S. M.; Bargar, J. R.; Janot, N.; Yabusaki, S.; Long, P. E. Geochemical and mineralogical investigation of uranium in multi-element contaminated, organic-rich subsurface sediment. *Appl. Geochem.* **2014**, *42*, 77−85.

(6) U.S. DOE Grand Junction Office. *Final Site Observational Work Plan for the UMTRA Project Old Rifle Site*; 1999.

(7) Anderson, R. T.; Vrionis, H. A.; Ortiz-bernad, I.; Resch, C. T.; Long, P. E.; Dayvault, R. D.; Karp, K.; Marutzky, S.; Metzler, D. R.; Peacock, A. D.; White, D. C.; Lowe, M.; Lovley, D. R. Stimulating the in situ activity of *Geobacter* species to remove uranium from the groundwater of a uranium-contaminated aquifer. *Appl. Environ. Microbiol.* **2003**, *69* (10), 5884−5891.

(8) Yabusaki, S. B.; Fang, Y.; Long, P. E.; Resch, C. T.; Peacock, A. D.; Komlos, J.; Jaffé, P. R.; Morrison, S. J.; Dayvault, R. D.; White, D. C.; Anderson, R. T. Uranium removal from groundwater via in situ biostimulation: Field-scale modeling of transport and biological processes. *J. Contam. Hydrol.* **2007**, *93* (1−4), 216−235.

(9) U.S. DOE Legacy Management. *Rifle, Colorado, Processing Sites and Disposal Site - Fact Sheet*; 2011.

(10) Qafoku, N. P.; Kukkadapu, R. K.; McKinley, J. P.; Arey, B. W.; Kelly, S. D.; Wang, C.; Resch, C. T.; Long, P. E. Uranium in framboidal pyrite from a naturally bioreduced alluvial sediment. *Environ. Sci. Technol.* **2009**, *43* (22), 8528−8534.

(11) Prietzel, J.; Thieme, J.; Tyufekchieva, N.; Paterson, D.; McNulty, I.; Kögel-Knabner, I. Sulfur speciation in well-aerated and wetland soils in a forested catchment assessed by sulfur K-edge X-ray absorption near-edge spectroscopy (XANES). *J. Plant Nutr. Soil Sci.* **2009**, *172* (3), 393−403.

(12) Druhan, J. L.; Steefel, C. I.; Conrad, M. E.; DePaolo, D. J. A large column analog experiment of stable isotope variations during




DOI: 10.1021/acs.est.5b03208
*Environ. Sci. Technol.* 2016, 50, 46−53

reactive transport: I. A comprehensive model of sulfur cycling and δ34S fractionation. *Geochim. Cosmochim. Acta* **2014**, *124*, 366−393.
(13) Wei, D.; Osseo-Asare, K. Aqueous synthesis of finely divided pyrite particles. *Colloids Surf., A* **1997**, *121* (1), 27−36.
(14) Rickard, D. T.; Luther, G. W. Chemistry of iron sulfides. *Chem. Rev.* **2007**, *107* (2), 514−562.
(15) Burton, E. D.; Bush, R. T.; Sullivan, L. A.; Hocking, R. K.; Mitchell, D. R. G.; Johnston, S. G.; Fitzpatrick, R. W.; Raven, M. D.; McClure, S.; Jang, L. Y. Iron-monosulfide oxidation in natural sediments: resolving microbially mediated S transformations using XANES, electron microscopy, and selective extractions. *Environ. Sci. Technol.* **2009**, *43* (9), 3128−3134.
(16) Lezama-Pacheco, J. S.; Cerrato, J. M.; Veeramani, H.; Alessi, D. S.; Suvorova, E.; Bernier-Latmani, R.; Giammar, D. E.; Long, P. E.; Williams, K. H.; Bargar, J. R. Long-term in situ oxidation of biogenic uraninite in an alluvial aquifer: Impact of dissolved oxygen and calcium. *Environ. Sci. Technol.* **2015**, *49* (12), 7340−7347.
(17) Burton, E. D.; Bush, R. T.; Johnston, S. G.; Sullivan, L. A.; Keene, A. F. Sulfur biogeochemical cycling and novel Fe−S mineralization pathways in a tidally re-flooded wetland. *Geochim. Cosmochim. Acta* **2011**, *75* (12), 3434−3451.
(18) Zeng, T.; Arnold, W. A.; Toner, B. M. Microscale characterization of sulfur speciation in lake sediments. *Environ. Sci. Technol.* **2013**, *47* (3), 1287−1296.
(19) Couture, R.-M.; Wallschläger, D.; Rose, J.; Van Cappellen, P. Arsenic binding to organic and inorganic sulfur species during microbial sulfate reduction: a sediment flow-through reactor experiment. *Environ. Chem.* **2013**, *10* (4), 285.
(20) Bargar, J. R.; Williams, K. H.; Campbell, K. M.; Long, P. E.; Stubbs, J. E.; Suvorova, E. I.; Lezama-Pacheco, J. S.; Alessi, D. S.; Stylo, M.; Webb, S. M.; Davis, J. A.; Giammar, D. E.; Blue, L. Y.; Bernier-Latmani, R. Uranium redox transition pathways in acetate-amended sediments. *Proc. Natl. Acad. Sci. U. S. A.* **2013**, *110* (12), 4506−4511.
(21) Hyun, S. P.; Davis, J. a.; Sun, K.; Hayes, K. F. Uranium(VI) reduction by iron(II) monosulfide mackinawite. *Environ. Sci. Technol.* **2012**, *46* (6), 3369−3376.
(22) Senko, J. M.; Istok, J. D.; Suflita, J. M.; Krumholz, L. R. In-situ evidence for uranium immobilization and remobilization. *Environ. Sci. Technol.* **2002**, *36* (7), 1491−1496.
(23) Istok, J. D.; Senko, J. M.; Krumholz, L. R.; Watson, D.; Bogle, M. A.; Peacock, A.; Chang, Y.-J.; White, D. C. In situ bioreduction of technetium and uranium in a nitrate-contaminated aquifer. *Environ. Sci. Technol.* **2004**, *38* (2), 468−475.
(24) Moon, H. S.; Komlos, J.; Jaffé, P. R. Uranium reoxidation in previously bioreduced sediment by dissolved oxygen and nitrate. *Environ. Sci. Technol.* **2007**, *41* (13), 4587−4592.
(25) Moon, H. S.; Komlos, J.; Jaffé, P. R. Biogenic U(IV) oxidation by dissolved oxygen and nitrate in sediment after prolonged U(VI)/Fe(III)/SO(4)(2-) reduction. *J. Contam. Hydrol.* **2009**, *105* (1−2), 18−27.
(26) Carpenter, J.; Bi, Y.; Hayes, K. F. Influence of iron sulfides on abiotic oxidation of UO2 by nitrite and dissolved oxygen in natural sediments. *Environ. Sci. Technol.* **2015**, *49*, 1078−1085.
(27) Williams, K. H.; Bargar, J. R. A Floodplain perspective on elemental cycling and uranium plume persistence. In *Goldschmidt Conference*, 2014.
(28) Nolan, J.; Weber, K. A. Natural uranium contamination in major U.S. aquifers linked to nitrate. *Environ. Sci. Technol. Lett.* **2015**, *2* (8), 215−220.
(29) Gurwick, N. P.; Groffman, P. M.; Yavitt, J. B.; Gold, A. J.; Blazejewski, G. A.; Stolt, M. H. Microbially available carbon in buried riparian soils in a glaciated landscape. *Soil Biol. Biochem.* **2008**, *40* (1), 85−96.
(30) Blazejewski, G. A.; Stolt, M. H.; Gold, A. J.; Gurwick, N. P.; Groffman, P. M. Spatial distribution of carbon in the subsurface of riparian zones. *Soil Sci. Soc. Am. J.* **2009**, *73* (5), 1733.
(31) Ricker, M. C.; Stolt, M. H.; Donohue, S. W.; Blazejewski, G. A.; Zavada, M. S. Soil organic carbon pools in riparian landscapes of southern New England. *Soil Sci. Soc. Am. J.* **2013**, *77* (3), 1070.
(32) Chaopricha, N. T.; Marín-Spiotta, E. Soil burial contributes to deep soil organic carbon storage. *Soil Biol. Biochem.* **2014**, *69*, 251−264.
(33) Elliott, J. G.; Hammack, L. A. Entrainment of riparian gravel and cobbles in an alluvial reach of a regulated canyon river. *River Res. Appl.* **2000**, *16* (1), 37−50.
(34) Van Steeter, M. M.; Pitlick, J. Geomorphology and endangered fish habitats of the upper Colorado River: 1. Historic changes in streamflow, sediment load, and channel morphology. *Water Resour. Res.* **1998**, *34* (2), 287.
(35) Fang, Y.; Yabusaki, S. B.; Morrison, S. J.; Amonette, J. P.; Long, P. E. Multicomponent reactive transport modeling of uranium bioremediation field experiments. *Geochim. Cosmochim. Acta* **2009**, *73* (20), 6029−6051.
(36) Yabusaki, S. B.; Fang, Y.; Williams, K. H.; Murray, C. J.; Ward, A. L.; Dayvault, R. D.; Waichler, S. R.; Newcomer, D. R.; Spane, F. A.; Long, P. E. Variably saturated flow and multicomponent biogeochemical reactive transport modeling of a uranium bioremediation field experiment. *J. Contam. Hydrol.* **2011**, *126* (3−4), 271−290.


DOI: 10.1021/acs.est.5b03208
*Environ. Sci. Technol.* 2016, 50, 46−53